Crystal structure and superionic conductivity of PbF_2 doped with KF

1998 J. Phys.: Condens. Matter 10 8429

(http://iopscience.iop.org/0953-8984/10/38/005)

J. Phys.: Condens. Matter **10** (1998) 8429–8446. Printed in the UK PII: S0953-8984(98)94865-2

Crystal structure and superionic conductivity of PbF_2 doped with KF

S Hull†‖, P Berastegui†, S G Eriksson‡ and N J G Gardner§

† The ISIS Facility, Rutherford Appleton Laboratory, Didcot, Oxfordshire, OX11 0QX, UK
‡ Studsvik Neutron Research Laboratory, S-611 82 Nykoping, Sweden
§ Oxford Physics, Clarendon Laboratory, Parks Road, Oxford, OX1 3PU, UK

Received 8 June 1998

Abstract. The crystal structure and ionic conductivity of polycrystalline samples of $(PbF_2)_{1-x}$-$(KF)_x$ with $0 \leqslant x \leqslant 0.333$ are investigated using neutron diffraction and impedance spectroscopy techniques. The maximum solid solubility of KF in the fluorite structured β-PbF_2 is found to be $x = 0.013(6)$. However, the introduction of K^+ and the associated charge compensating anion vacancies has a dramatic effect on the ambient temperature ionic conductivity, which increases by a factor $5.6(2) \times 10^3$ for an $x = 0.01$ sample at 350 K. At higher dopant levels the ambient temperature conductivity falls steadily in the range $0.05 \leqslant x \leqslant 0.333$ due to the presence of an increasing volume fraction of relatively poorly conducting additional phases, apparently comprising orthorhombic α-PbF_2 and a further phase of probable composition $PbKF_3$. However, the ionic conductivity of these samples show an abrupt increase at $T = 520(5)$ K, as the two minority phases react to form a single, superionic phase. Within this high-temperature modification the anions are dynamically disordered over the tetrahedral and, to a lesser extent, the octahedral interstices created by a body centred cubic (bcc) cation sublattice formed by Pb^{2+} and K^+. This phase is, therefore, an example of an *anion* conducting bcc superionic and its structure is 'anti-' to that adopted by the archetypal superionic phase α-AgI. A plausible model describing the structural relationship between these two anti-types, including the short-range order between mobile ions within the bcc-$(Pb_{1-x}K_x)F_{2-x}$ phase, is given.

1. Introduction

Superionics are materials which display exceptionally high values of ionic conductivity (typically $\sigma \sim 1\ \Omega^{-1}\ cm^{-1}$) whilst in the solid state. Two of the most widely studied families of superionic compounds are the Ag^+ and Cu^+ conductors and the group of ionic compounds which adopt the fluorite structure (space group $Fm\bar{3}m$) [1]. Examples of the former are AgI, Ag_2Te and CuI, and the transition from the 'normal' (insulating) state to the superionic state is abrupt (a type I transition in the notation of Boyce and Huberman [2]) and associated with a first-order structural phase transition. The high-temperature phase is characterized by extensive cation disorder, with mobile Ag^+ or Cu^+ performing rapid hops between the interstitial sites formed by an essentially rigid anion sublattice. This is body-centred cubic (bcc) in the case of α-AgI [3, 4], α-CuBr [5] and γ-Ag_2Te [6] and face-centred cubic (fcc) in α-CuI [5, 7] and γ-Ag_2Te [6]. The bcc structured compounds generally have higher values of ionic conductivity than the fcc ones, probably because the migrating species preferentially favour four-fold coordination and the number of available tetrahedral

‖ E-mail address: sh@isise.rl.ac.uk.

0953-8984/98/388429+18$19.50

interstices is higher in the case of a bcc sublattice (12) than an fcc one (four) [2]. In contrast, the fluorite structured compounds such as CaF_2, $SrCl_2$ and β-PbF_2, undergo a gradual build up of dynamic anion Frenkel disorder on increasing temperature (type II superionic) [8]. This intrinsic, thermally induced disorder produces a rapid, though continuous, increase in the ionic conductivity, σ, a λ-type anomaly in the specific heat C_p [9] and a peak in the lattice expansivity α_V [10]. The superionic transition (generally defined to be the temperature of the peak in C_p) is typically $T_c \sim 0.7$–$0.8\ T_m$, where T_m is the melting temperature.

Of these fluorite structured compounds, β-PbF_2 has attracted considerable attention because it has the lowest transition temperature, both in absolute ($T_c \sim 710$ K) and relative ($T_c/T_m \sim 0.65$) terms [11]. However, the material is complicated by the presence of the cotunnite structured α phase (space group $Pnma$), to which fluorite structured β-PbF_2 transforms at a relatively modest pressure ($\sim$0.4 GPa) [12]. Upon release of pressure, α-PbF_2 is retained as a metastable phase indefinitely and the reverse $\alpha \rightarrow \beta$ transformation can only be achieved by heating to over 610 K. Potential applications of PbF_2 in battery technologies require that the superionic transition temperature T_c be reduced as far as possible, thereby enhancing the ionic conductivity at temperatures close to ambient. In addition, the $\beta \rightarrow \alpha$ transition pressure should be increased, because α-PbF_2 would tend to be produced by grinding and/or compacting during device manufacture and it is a relatively poor conductor [13]. Extensive studies using chemical doping to bring about the desired changes in the p–T phase diagram of PbF_2 have been performed, including the introduction of monovalent (i.e. K^+ [14, 15] and Ag^+ [16]), divalent (i.e. Sn^{2+} [17]), trivalent (i.e. Bi^{3+} [18], Y^{3+} [19] and S^{3+} [20]) and tetravalent (i.e. Zr^{4+} [21] and Th^{4+} [22, 23]) cation species.

In this paper we consider the effects of KF doping on the structure and ionic conductivity of PbF_2 in the range $0 \leqslant x \leqslant 0.333$. At low dopant concentrations ($x <\sim 0.01$) the potassium cations sit substitutionally on the host fluorite Pb^{2+} sites and electrical neutrality is maintained by the formation of F^- vacancies on the anion sublattice [14, 24]. These extrinsic defects have a dramatic effect on the room temperature ionic conductivity, which increases by over three orders of magnitude at $x = 0.01$ [24]. However, the behaviour of the doped material at higher KF contents is less clear, largely due to ambiguities in the $(PbF_2)_{1-x}$-$(KF)_x$ binary phase diagram (see [25–27]). In particular, the extent of the fluorite structured solid solution is unclear and there have been conflicting reports concerning the nature of the ordered phases present, including evidence for $x = 0.5$ ($PbKF_3$) and $x = 0.8$ (PbK_4F_6) stoichiometries. As a consequence, the inter-relationship between the extrinsic defects (caused by aliovalent doping) and the intrinsic (thermally induced) lattice disorder is not well understood.

2. Experimental

2.1. Sample preparation

$(PbF_2)_{1-x}$-$(KF)_x$ samples with $x = 0.01$, 0.05, 0.10, 0.25, 0.30 and 0.333 were prepared by mixing the appropriate amounts of PbF_2 (99.997% purity, Alfa Products) and KF (99.994% purity, Alfa Products) and grinding using an agate mortar. The reactants had previously been dried overnight at 590 K. The samples were then sintered for 15 h at temperatures between 650 K and 890 K. Slow cooling at 30 K h^{-1} was necessary in order to obtain crystalline samples. All reactions were carried out in gold crucibles under a flowing nitrogen atmosphere and the samples handled in a nitrogen filled dry box. The melting point of the $x = 0.333$ sample was observed as 840(5) K in a nitrogen atmosphere.

2.2. Impedance spectroscopy

Two terminal measurements of the ionic conductivity were performed using a pelleted sample of 6 mm diameter and 5–6 mm length. These were held between two spring loaded platinum disks inside a boron nitride cell which is inserted into the hotzone of a horizontal tube furnace. Details of this device can be found elsewhere [28]. Complex impedance measurements were performed approximately every 3 min whilst the furnace temperature was first heated and then cooled at a constant rate of 60 K h^{-1}. A PC controlled Solartron S1260 frequency response analyser determined the conventional Z–Z' impedance plot over the frequency range from 0.1 Hz to 10 MHz. The real component of the sample impedance Z_S was determined using the program IMMFIT [28]. All measurements were performed under dynamic vacuum of $\sim 10^{-2}$ Pa and temperature monitoring obtained using chromel–alumel thermocouples located within the cell at a distance of $\sim$2 mm from the sample pellet.

2.3. Neutron diffraction

Neutron diffraction experiments were performed using the Polaris powder diffractometer at the ISIS facility, Rutherford Appleton Laboratory, UK [29]. Time constraints restricted these investigations to the samples with $x = 0.10$, 0.30 and 0.333. Comparison data for pure $x = 0.00$ β-PbF_2 were taken from a previous study [10]. The samples were encapsulated inside thin walled vanadium cans of 11 mm diameter and 40 mm height. High-temperature measurements used a special furnace designed for neutron diffraction constructed of vanadium foil resistive heating element and heat shields. Diffraction data were predominantly collected using the backscattering detector bank which covers the scattering angles $130^\circ < \pm 2\theta < 160^\circ$ and provides data over the d-spacing range $0.2 < d(\text{Å}) < 3.2$ with a resolution $\Delta d/d \sim 5 \times 10^{-3}$. Additional information describing the variation with d-spacing of the coherent diffuse scattering was provided by measurements using the low-angle detector bank. These are situated at $28^\circ < \pm 2\theta < 42^\circ$, providing access to a wider d-spacing range $0.5 < \text{d(Å)} < 8.3$, though with a poorer resolution of $\Delta d/d \sim 10^{-2}$.

Analysis of the neutron diffraction data considered both the Bragg scattering, which gives the *time-averaged* distribution of ion positions within the unit cell, and the coherent diffuse scattering (observed as undulations of the measured 'background' between the Bragg peaks), which arises from short-range *instantaneous* correlations between disordered ions. The former were treated using the conventional Rietveld profile refinement of the normalized diffraction data, using the program TF12LS [30] based on the Cambridge crystallographic subroutine library [31]. In all cases the fitted parameters included an overall scale factor, a number of coefficients (usually 5) of a polynomial expression describing the background shape and a Gaussian width parameter describing the observed peak width. Details of the structural parameters included in the fitting procedure are discussed more fully below, as these are dependent on the nature of the particular phase under investigation. The mathematical expressions used to calculate the d-spacing variation of the diffuse scattering intensity using assumed defect models can be found elsewhere [32]. The coherent neutron scattering lengths of the constituent elements are given in table 1.

3. Results

3.1. Ionic conductivity

The variation of the ionic conductivity σ of the $(PbF_2)_{1-x}(KF)_x$ samples with KF concentration x is shown in figure 1 for representative temperatures of 350 K, 580 K and

Table 1. The values of the coherent neutron scattering length b and ionic radius r for Pb^{2+}, K^+ and F^- used in this study.

Ionic species	Coherent neutron scattering length b (fm)	Ionic radius r (Å)
Pb^{2+}	9.405	0.98
K^+	3.670	1.37
F^-	5.654	1.31

700 K. At the lowest of these temperatures σ rises very rapidly with KF concentration x, such that $\sigma_{350\ K} = 3.5(1) \times 10^{-3}\ \Omega^{-1}\ cm^{-1}$ for the $x = 0.01$ sample compared to $\sigma_{350\ K} = 6.4(2) \times 10^{-7}\ \Omega^{-1}\ cm^{-1}$ for the pure β-PbF_2 material. This is in agreement with previous measurements on this system [24]. At the higher dopant concentrations with $x > 0.05$ there is a steady decrease in $\sigma_{350\ K}$, falling to a value of $6.3(1) \times 10^{-5}\ \Omega^{-1}\ cm^{-1}$ at $x = 0.333$. A crude extrapolation of the two regions of $\log_{10}\sigma$ against x implies a discontinuity in the conduction mechanism at $x \sim 0.015$. However, further discussion of its origin will be deferred until after the presentation of the neutron diffraction measurements in the following subsection. At higher temperatures, the variation of σ with x is less marked and, in contrast to 350 K, $\sigma_{580\ K}$ and $\sigma_{700\ K}$ both increase with x over the entire range $0.0 \leqslant x \leqslant 0.333$.

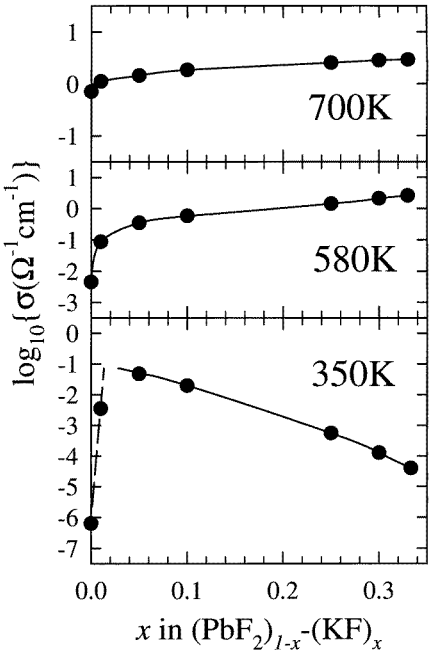

Figure 1. Variation of the ionic conductivity $\log_{10}\sigma$ with K^+ concentration x at temperatures of 350 K, 580 K and 700 K. The lines are guides to the eye, with the exception of the broken (low-x) line in the lower figure (350 K data) which represents the results of [24]. The abrupt change in the variation of $\sigma_{350\ K}$ with x indicates the solubility limit of K^+ in fluorite structured β-$(Pb_{1-x}K_x)F_{2-x}$ at $x \sim 0.015$.

These effects become clearer by consideration of the temperature dependence of the $x = 0.0$, 0.01, 0.10 and 0.30 samples in figure 2. The pure $x = 0.0$ β-PbF_2 sample shows the 'classic' type II superionic behaviour, with the ionic conductivity saturating at a temperature ~800 K and in accord with previous measurements [11]. On increasing temperature, the ionic conductivity of the $x = 0.01$ sample approaches that of the pure $x = 0.0$ material, presumably because the low concentration of extrinsic defects becomes

dominated by the extensive intrinsic (thermally induced) Frenkel disorder at $T >\sim 600$ K. However, the $x = 0.10$ and, to a greater extent, the $x = 0.30$ samples show abrupt increases in their ionic conductivity at $T = 520(5)$ K. In the latter case, σ jumps by $\sim 50\times$, reaching a value of 0.42(1) Ω^{-1} cm^{-1} at 580 K, approximately four orders of magnitude higher than the pure β-PbF_2 at the same temperature.

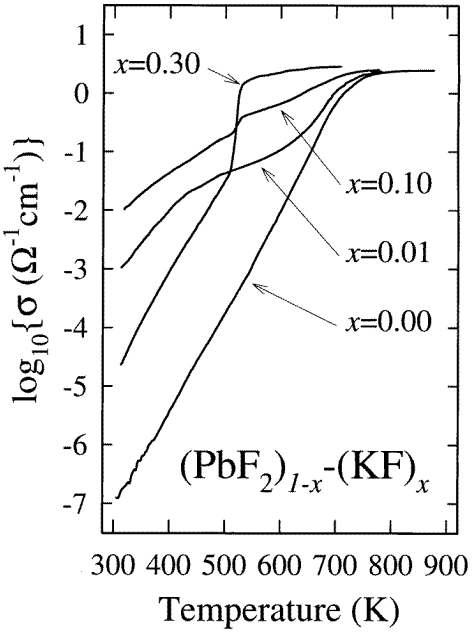

Figure 2. Variation of the ionic conductivity $\log_{10}\sigma$ with temperature for $(PbF_2)_{1-x}$-$(KF)_x$ samples with $x = 0.0$, 0.01, 0.10 and 0.30.

3.2. Neutron diffraction $x = 0.10$ sample

The evolution of the powder neutron diffraction pattern for the $x = 0.10$ sample is illustrated in figure 3. At all temperatures, the measured diffraction pattern is dominated by intense reflections at positions expected for the fluorite structured β phase. However, at ambient temperature there are additional weak reflections observed at, for example, $d = 1.64$ Å, 1.90 Å, 2.32 Å and 2.38 Å. These disappear at $T \sim 520$ K, to be replaced by another series of fewer, though marginally more intense, Bragg reflections. Further discussion of these features will be given in section 3.4.

We begin by performing time-of-flight Rietveld refinement of the dominant fluorite structured phase using the ambient temperature diffraction data. We refer to this phase as β-$(Pb_{1-y}K_y)F_{2-y}$ to denote that the K^+ content y is not necessarily equal to the compositional value x. Those regions of the time-of-flight diffraction pattern containing the weak additional reflections were excluded from the fitting procedure to avoid possible adverse effects on the refined parameter values. In the cubic fluorite structure (space group $Fm\bar{3}m$), the cations are located on the 4(a) Wyckoff sites at $(0, 0, 0) + fc$ (where fc denotes the face-centre translations $+(0, \frac{1}{2}, \frac{1}{2})$, $+(\frac{1}{2}, 0, \frac{1}{2})$ and $+(\frac{1}{2}, \frac{1}{2}, 0)$) and the anions are situated on the 8(c) sites at $(\frac{1}{4}, \frac{1}{4}, \frac{1}{4})+fc$ and $(\frac{1}{4}, \frac{1}{4}, \frac{3}{4})+fc$. The fitted structural parameters comprised the cubic lattice parameter a_0, the cation and anion isotropic thermal vibration parameters ($B_{Pb/K}$ and B_F) and the K^+ content y. The cation site was constrained to have full occupancy (but variable Pb^{2+}/K^+ ratio) with the F^- site value constrained to maintain overall electrical

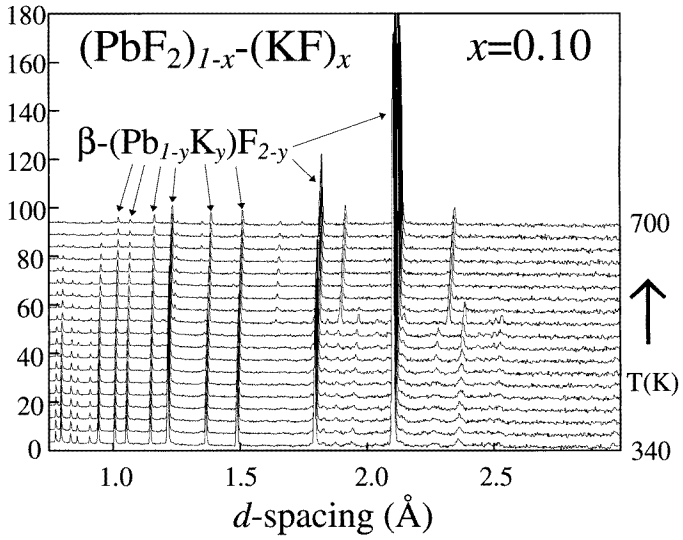

Figure 3. The evolution of the neutron diffraction pattern of the $(PbF_2)_{1-x}$-$(KF)_x$ $x = 0.10$ sample with temperature. The data shown cover the range $340 \leqslant T(K) \leqslant 700$ in 20 K steps. At all temperatures the pattern is dominated by the fluorite structured phase labelled β-$(Pb_{1-y}K_y)F_{2-y}$.

neutrality within the sample. The fitted parameters are listed in table 2, together with the corresponding values of a_0, B_{Pb} and B_F for a pure β-PbF_2 sample. Unfortunately, neutron (and x-ray) diffraction are relatively insensitive to the doping of KF into PbF_2, since the process reduces the mean scattering power of both the cation site (see table 1) and the anion site (via the formation of F^- vacancies). However, it is clear from table 2 that the refined value for the K content ($y = 0.013(6)$) is significantly less than that predicted solely from the chemical composition ($x = 0.10$). In addition, the relatively small difference between the lattice parameters a_0 for the pure and doped compounds is inconsistent with that expected by the introduction of the larger potassium ion [15]. These observations are, therefore, indicative of phase segregation, such that

$(PbF_2)_{1-x}(KF)_x \qquad x = 0.10 \rightarrow$ fluoriteβ-$(Pb_{1-y}K_y)F_{2-y}$

with $y = 0.013(6)$ + higher K^+content phase(s).

We now briefly consider the effect of temperature on the former phase, to investigate the influence of the (limited) K^+ doping on the superionic transition. The nature of the higher K^+ content phase(s) will be addressed later. The analysis strategy closely followed that adopted in our previous investigation of the structural behaviour of pure β-PbF_2 [10]. The fitted structural parameters were the cubic lattice parameter a_0, isotropic thermal vibration parameters for the cation and anion species, $B_{Pb/K}$ and B_F, and the fraction of fluorine ions which leave the regular lattice sites, n_V. The results of these refinements are illustrated in figure 4. The lattice parameter clearly shows the presence of an anomalous increase in the expansivity da_0/dT in the region ~700 K. This effect has been observed in pure β-PbF_2 and is associated with the onset of the thermally induced Frenkel disorder which characterizes the superionic state [10]. Similarly, the concentration of anions leaving the regular lattice sites to form Frenkel interstitials appears very similar in the pure $y = 0.0$ and K^+ doped $y = 0.013(6)$ samples. The introduction of the limited K^+ dopant into β-PbF_2 has, therefore, little effect on the transition to the superionic state with this fluorite structured material.

Table 2. Results of the analysis of the ambient temperature data for pure β-PbF_2 and the β-$(Pb_{1-y}K_y)F_{2-y}$ phase observed in the $(PbF_2)_{1-x}$-$(KF)_x$ sample with $x = 0.10$.

Sample	Pure β-PbF_2	β-$(Pb_{1-y}K_y)F_{2-y}$ phase in $(PbF_2)_{1-x}(KF)_x$ $x = 0.10$ sample
Temperature	295(2) K	295(2) K
Space group	$Fm\bar{3}m$	$Fm\bar{3}m$
Formula units per unit cell	$Z = 4$	$Z = 4$
Unit cell constant	$a_0 = 5.9463(1)$ Å	$a_0 = 5.9469(1)$ Å
Cations	4(a) sites at $(0, 0, 0) + fc$ $B_{Pb} = 0.52(2)$ Å^2	4(a) sites at $(0, 0, 0) + fc$ $B_{Pb/K} = 0.55(2)$ Å^2 $y = 0.013(6)$ $\Rightarrow m_{Pb} = Z(1 - y) = 3.95(2)$ $\Rightarrow m_K = Z_y = 0.05(2)$
Anions	8(c) sites at $\pm(\frac{1}{4}, \frac{1}{4}, \frac{1}{4}) + fc$ $B_F = 0.83(3)$ Å^2	8(c) sites at $\pm(\frac{1}{4}, \frac{1}{4}, \frac{1}{4}) + fc$ $B_F = 0.94(4)$ Å^2 $\Rightarrow m_F = Z(2 - y) = 7.95(2)$
Goodness-of-fit	$\chi^2 = 1.10$ 3753 experimental data points 113 Bragg peaks 10 fitted parameters	$\chi^2 = 1.22$ 3760 experimental data points 113 Bragg peaks 11 fitted parameters

3.3. Neutron diffraction: $x = 0.30$ sample

Inspection of the room temperature neutron diffraction pattern from the $x = 0.30$ sample (figure 5) confirms that the minority phase with higher K^+ content observed in the $x = 0.10$ sample is now the dominant one. Conversely, only a few, very weak reflections arising from the fluorite structured phase are now present. Presumably the latter is β-$(Pb_{1-y}K_y)F_{2-y}$ with the maximum solubility of $y = 0.013(6)$ discussed in the previous section and no further analysis of its temperature dependence was attempted. Extrapolation of the decrease in intensity of the β-$(Pb_{1-y}K_y)F_{2-y}$ Bragg peaks with total K^+ content x suggests that the fluorite structured phase is absent at $x = 0.333$. This was subsequently confirmed by neutron diffraction investigations of a $(PbF_2)_{1-x}$-$(KF)_x$ sample with $x = 0.333$. The exact structural nature of this material is discussed in the following subsection.

3.4. Ambient temperature structure: $x = 0.333$ sample

The diffraction pattern collected from the ambient temperature phase of the $(PbF_2)_{1-x}$-$(KF)_x$ sample with $x = 0.333$ is extremely complex. The observed d-spacings are listed in table 3. Unfortunately, attempts to determine the structure of this phase at ambient temperature *ab initio* have not been successful. However, a number of the observed d-spacings are very similar to those observed in cotunnite structured α-PbF_2 (table 3). There are two possible explanations for this feature. First, the sample with $x = 0.333$ could be a single phase of composition Pb_2KF_5 and possess a superstructure of α-PbF_2. The latter could be the result of ordering of the two cation species and/or ordering of the anion vacancies. However, simulations of the diffraction patterns using the structures of related compounds with the same stoichiometry (such as Pb_2TlCl_5 [33], Pd_2CsF_5 [34] and Sn_2KF_5 [35]) show no similarity to that measured. Furthermore, no phase of this composition has been identified in the published phase diagrams of the PbF_2-KF system [25–27]. Alternatively, it is possible that the material exists as a mixture of two phases, α-PbF_2 and a further phase of higher KF content. In

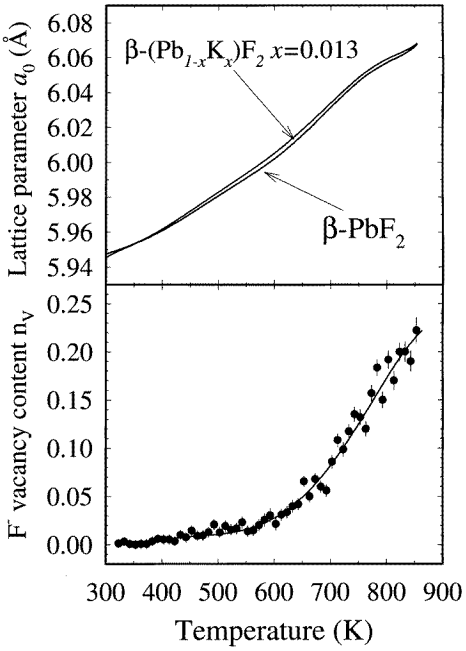

Figure 4. Comparison of the structural properties of pure β-PbF_2 and the doped fluorite structured phase β-$(Pb_{1-y}K_y)F_{2-y}$ present in the $(PbF_2)_{1-x}$-$(KF)_x$ sample with $x = 0.10$. The close similarity between their thermal expansions, including the anomalous behaviour close to the superionic transition at $T \sim 700$ K (top), indicates that doping has relatively little influence on the intrinsic Frenkel disorder. This is confirmed in the bottom figure by the defect concentrations for the doped sample (●) and the pure material (line taken from [10]).

support of this hypothesis, $PbKF_3$ has been identified [26], but no details of its structure have been reported. Attempts to determine a unit cell using only those d-spacings not consistent with α-PbF_2 (table 3) proved unsuccessful and further investigations to resolve the structural description of $(PbF_2)_{1-x}$-$(KF)_x$ with $x = 0.333$ at ambient temperature are planned, including the use of high $\Delta d/d$ resolution diffraction data collected with both neutron and x-ray radiations. However, of principal concern in this paper is the abrupt increase in the ionic conductivity at $T = 520(5)$ K. With reference to figure 5, it is clear that this transition to a superionic phase is coincident with a dramatic simplification of the neutron diffraction pattern.

3.5. High temperature structure: $x = 0.333$ sample

The structural investigations of the high temperature superionic phase of $(PbF_2)_{1-x}$-$(KF)_x$ with $x = 0.333$ used diffraction data collected at 673 K. As illustrated in figure 5, the high temperature diffraction pattern is extremely sparse. The observed peaks can be indexed on a body-centred cubic (bcc) unit cell with $a = 4.6655(1)$ Å. This is in broad agreement with Schmitz-Dumont and Bergerhoff [25], who observed a minority phase with $a = 4.64$ Å in a sample with $x = 0.25$. Furthermore, the rapid fall-off in intensity at short d-spacings and the diffuse scattering observed as modulations in the measured background between the Bragg peaks are indicative of a highly disordered phase. This is consistent with the high-measured value of σ (figure 1) and suggest that the $x = 0.333$ sample becomes a single bcc structured superionic phase, of the type observed in the cation disordered phases

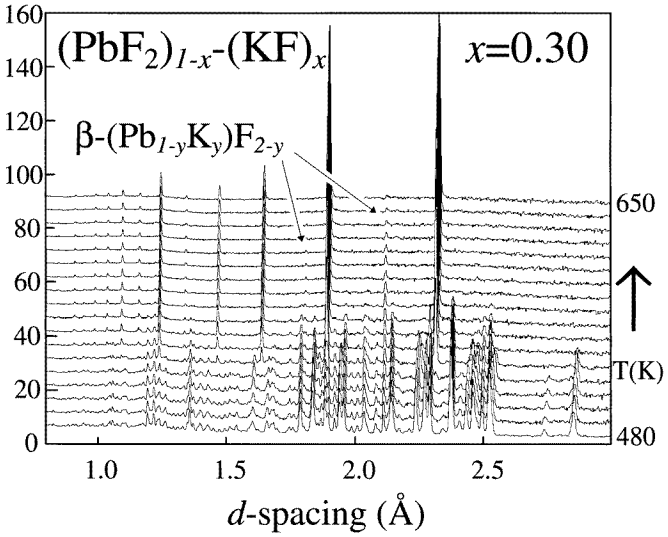

Figure 5. The evolution of the neutron diffraction pattern of the $(PbF_2)_{1-x}$-$(KF)_x$ $x = 0.30$ sample with temperature. The data shown cover the range $480 \leqslant T(\mathrm{K}) \leqslant 650$ in 10 K steps. The transition to the superionic bcc-$(Pb_{1-x}K_x)F_{2-x}$ phase with $x = 0.333$ at $T = 620(5)$ K is clearly visible. A small quantity of the fluorite structured phase β-$(Pb_{1-y}K_y)F_{2-y}$ is also present at all temperatures.

such as α-AgI [3, 4], α-CuBr [5] and γ-Ag_2Te [6]. For reasons that will become apparent subsequently, we denote this phase bcc-$(Pb_{1-x}K_x)F_{2-x}$. The fluorite structured superionic phase of pure β-PbF_2 is characterized by extensive *anion* disorder [10] and it is reasonable to assume that bcc-$(Pb_{1-x}K_x)F_{2-x}$ with $x = 0.333$ is 'anti-' to the cation conducting phases discussed earlier. Figure 6 shows a schematic representation of such a bcc structured superionic phase. The 'fixed' ions (Pb^{2+} and K^+ in bcc-$(Pb_{1-x}K_x)F_{2-x}$ and I^- in α-AgI) are located in the 2(a) sites of space group $Im\bar{3}m$ at $(0, 0, 0)$ and $(\frac{1}{2}, \frac{1}{2}, \frac{1}{2})$. The mobile ions ($F^-$ in bcc-$(Pb_{1-x}K_x)F_{2-x}$ and Ag^+ in α-AgI) diffuse through the bcc sublattice and can occupy the various interstitial cavities which are labelled according to their surrounding environment of unlike neighbours. As summarized in table 4, these are the octahedral 6(b) sites at $(0, \frac{1}{2}, \frac{1}{2})$ etc, the tetrahedral 12(d) sites at $(\frac{1}{4}, 0, \frac{1}{2})$ etc, the trigonal 24(g) sites at $(w, 0, \frac{1}{2})$ etc., with $w = \frac{3}{8}$ and the linear 8(c) sites at $(\frac{1}{4}, \frac{1}{4}, \frac{1}{4})$ etc. However, in bcc-$(Pb_{1-x}K_x)F_{2-x}$, F^- occupying the latter would be situated at a distance $\sqrt{3}a/4 \sim 2.0$ Å from the cation sites and, in view of the ionic radii of the constituent ions (table 1), we do not consider these linear sites further.

On average, the unit cell contains $1.333 \times Pb^{2+}$ and $0.667 \times K^+$ distributed over the 2(a) sites. Any long-range order of these two species resulting from a non-random distribution of cations would lower the symmetry from $Im\bar{3}m$ to $Pm\bar{3}m$ and additional (hkl) Bragg peaks with $h + k + l \neq 2n$ would, in principle, be observed. The significant difference in the coherent neutron scattering lengths for Pb^{2+} and K^+ (table 1) gives a high sensitivity to such partial ordering and simulations of the diffraction pattern indicate that peaks such as (001) and (111) would be observable at the measured level of counting statistics for only a small deviation (∼5%) away from a complete random distribution. This justifies our use of the () parentheses in the bcc-$(Pb_{1-x}K_x)F_{2-x}$ label for this superionic phase.

Whilst the absence of these Bragg peaks in the experimental data discounts the presence of any long-range cation order it does not rule out the possibility of short-range correlations

Table 3. The observed d-spacing values at ambient temperature for the $(PbF_2)_{1-x}$-$(KF)_x$ sample with $x = 0.333$ illustrating the similarity to those calculated for orthorhombic α-PbF_2.

$(PbF_2)_{1-x}(KF)_x$ $x = 0.333$	Orthorhombic α-PbF_2	
d (Å)	d (Å)	hkl
6.3408	—	—
5.6223	—	—
5.5358	—	—
5.0290	—	—
4.8740	—	—
3.8356	3.8345	002
3.6753	—	—
3.4526	3.4543	011
3.3002	3.2958	102
3.2268	3.2240	200
3.1663	—	—
3.0492	3.0449	111
2.8331	—	—
2.7146	—	—
2.5116	2.5089	112
2.4809	2.4768	210
2.4459	—	—
2.4160	—	—
2.3878	2.3764	103
2.3588	2.3569	211
2.3198	—	—
2.2777	—	—
2.2539	—	—
2.2194	—	—
2.1648	—	—
2.1322	2.1328	013
2.0690	2.0696	301
2.0250	2.0249	113
1.9994	2.0031	203

on the scale of one or two unit cells. This question will be addressed further in section 4.3. Instead, we turn our attention to the anion locations. A total of $2(2-x) = 3.333$ anions in the unit cell can be distributed over the six octahedral, 12 tetrahedral and 24 trigonal sites. To determine the preferred locations of the highly disordered cations we fit structural models to the experimental data, allowing anions to occupy one or more of the interstitial sites (octahedral, tetrahedral and trigonal) using as criteria the usual goodness-of-fit χ^2 statistic, the stability of the least-squares minimization procedure (i.e. the absence of significant correlations between variables) and the requirement that the fitted parameters are physically sensible.

A summary of the different models and their results are given in table 5. We begin by performing a so-called 'model independent' fit to the data. This approach (labelled A) uses as variables the 20 coefficients of a polynomial expansion to fit the observed background, the unit cell parameter a_0, a Gaussian peak width parameter and 95 intensities of the Bragg peaks in the range 0.33 Å $< d <$ 3.10 Å. As such, it neither assumes nor provides any structural information. However, the resultant value of χ^2 (0.98) gives an estimate of the 'target' for subsequent structural analysis and confirms that all the peaks in the measured diffraction pattern are consistent with the chosen unit cell and space group symmetry. The relatively large number of parameters required to describe the background is required to

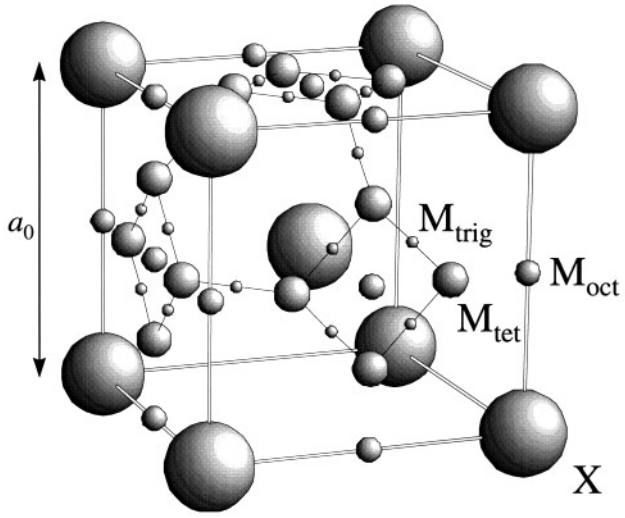

Figure 6. Schematic diagram of the structure of a bcc structured superionic phase of lattice parameter a_0. The large spheres represent the immobile X ions situated on the $(0, 0, 0)$ and $(\frac{1}{2}, \frac{1}{2}, \frac{1}{2})$ positions. Possible positions for the mobile M ions in the octahedral (M_{oct}), tetrahedral (M_{tet}) and trigonal (M_{trig}) interstices are shown.

Table 4. The four possible sites occupied by the mobile ions within a bcc structured superionic phase (space group $Im\bar{3}m$) of lattice parameter a_0.

Cation site	Wyckoff site	Position	Cation distances
Octahedral	6(b)	$(0, \frac{1}{2}, \frac{1}{2})$ etc	$\begin{cases} 2@\frac{a_0}{2} \\ 4@\frac{a_0}{\sqrt{2}} \end{cases}$
Tetrahedral	12(d)	$(\frac{1}{4}, 0, \frac{1}{2})$ etc	$4@\frac{\sqrt{5}a_0}{4}$
Trigonal	24(g)	$(w, 0, \frac{1}{2})$ etc with $w = \frac{3}{8}$	$3@\frac{\sqrt{18}a_0}{8}$
Linear	8(c)	$(\frac{1}{4}, \frac{1}{4}, \frac{1}{4})$ etc	$2@\frac{\sqrt{3}a_0}{4}$

adequately fit the undulating diffuse scattering observed in the superionic phase. In all the structural refinements (models B $\rightarrow$ H) the background parameters, unit cell constant and Gaussian width parameter are varied. In addition, the anion and cation thermal parameters ($B_{Pb/K}$ and B_F, respectively) were refined. In those cases where more than one interstitial site is considered, the thermal parameters for each site ($B_{F,oct}$, $B_{F,tet}$ and $B_{F,trig}$) were initially constrained to be equal but subsequently varied independently. In all cases the total fluorine content in the unit cell was held at the value given by the dopant concentration x (i.e. $m_{F,oct} + m_{F,tet} + m_{F,trig} = 2(2 - x) = 3.333$). All fits were started with the anions distributed uniformly over all the available sites in the model.

Models B, C and D consider the anions to only occupy the octahedral, tetrahedral and trigonal sites, respectively. These do not provide an acceptable fit to the experimental data ($\chi^2 > 4$) and, in addition, the fitted thermal vibration parameter for the octahedral site

Table 5. Summary of the structural models used to determine the structure of the high-temperature superionic phase bcc-$(Pb_{1-x}K_x)F_{2-x}$ with $x = 0.333$ See section 3.5 for an explanation of the symbols.

Model	Description	χ^2	Comments
A	Model independent fit	0.98	
B	Octahedral sites only	5.87	$B_{F,oct} = 51$ Å^2
C	Tetrahedral sites only	4.57	
D	Trigonal sites only	4.06	
E	Octahedral + tetrahedral sites	1.13	
F	Octahedral + trigonal sites	3.32	$m_{F,trig}$ small. Unstable if $B_{F,oct} \neq B_{F,tet}$
G	Tetrahedral + trigonal sites	2.60	$m_{F,trig}$ small. Unstable if $B_{F,oct} \neq B_{F,trig}$
H	Octahedral + tetrahedral + trigonal	1.07	$m_{F,trig}$ small.

(model B) has a physically unrealistic value of $B_{F,oct} = 51$ Å^2, corresponding to a mean thermal vibration $\langle u \rangle$ of $\sqrt{B_{F,oct}/8\pi} \sim 1.4$ Å. Models E, F and G allow two sites to be filled simultaneously but, as shown in table 5, only model E (octahedral and tetrahedral sites) provides a significant improvement in χ^2. Models F and G indicate relatively little fluorine occupancy of the trigonal sites ($m_{F,trig} < 0.5$). In addition, models F and G become highly unstable during attempts to vary the thermal parameters of the two sites independently, due to excessive correlations between the thermal vibration and occupation parameters. Finally, we consider a fit (model H) in which all sites can be occupied simultaneously. With the initial constraint of equal thermal vibration parameters ($B_{F,oct} = B_{F,tet} = B_{F,trig}$) the fit converges to a value close to that obtained in model E and with no significant occupancy of the trigonal sites. As expected, release of the thermal parameter constraint causes χ^2 to diverge.

We conclude that the best description of the experimental diffraction data for bcc-$(Pb_{1-x}K_x)F_{2-x}$ with $x = 0.333$ is provided by model E, with the fitted parameters listed in table 6. The quality of the final fit to the data is illustrated in figure 7. The final value of χ^2 is slightly higher than that provided by the model independent fit and probably represents approximations used in describing the highly disordered system in terms of discrete, well defined lattice positions. However, the increasing number of variables required to consider, for example, anisotropic and anharmonic thermal vibrations of the ions cannot be justified in view of the limited number of observed Bragg peaks.

4. Discussion

4.1. Overview

The ionic conductivity data for the fluorite structured solid solution region of $(PbF_2)_{1-x}$-$(KF)_x$ at $x < 0.013(6)$ presented in section 3.1 are in accord with the accepted model of dopant K^+ located substitutionally on the Pb^{2+} sites [24]. Electrical neutrality is maintained by the formation of vacancies on the anion sublattice and these vacancies give rise to a dramatic increase in the ionic conductivity (by $\sim 5 \times 10^3$, see figure 1). At elevated temperatures, it is interesting to consider the relationship between these vacancies and the intrinsic disorder which characterizes the transition to the superionic state. The direct comparison between the structural behaviour and the ionic conductivity of the doped fluorite solid solution β-$(PbF_2)_{1-x}(KF)_x$ with $x = 0.013(6)$ and pure β-PbF_2 (taken from reference [10]) in figures 2 and 4 indicate that the extrinsic defects (F^- vacancies) have little or no effect on the intrinsic (Frenkel) disorder. The concentration of Frenkel defects at $T \sim 700$ K

Table 6. Results of the analysis of the 673 K neutron diffraction data for the superionic phase bcc-$(Pb_{1-x}K_x)F_{2-x}$ with $x = 0.333$.

Sample	bcc-$(Pb_{1-x}K_x)F_{2-x}$ with $x = 0.333$
Temperature	673(2) K
Space group	$Im\bar{3}m$
Formula units per unit cell	$Z = 2$
Unit cell constant	$a_0 = 4.6655(1)$ Å
Cations	2(a) sites at (0, 0, 0) and ($\frac{1}{2}$, $\frac{1}{2}$, $\frac{1}{2}$)
	$B_{Pb/K} = 6.3(2)$ Å^2
Anions	12(d) sites at ($\frac{1}{4}$, 0, $\frac{1}{2}$) etc.
	$m_{F,tet} = 2.53(2)$
	$B_{F,tet} = 10.4(3)$ Å^2
	6(b) sites at (0, $\frac{1}{2}$, $\frac{1}{2}$) etc.
	$m_{F,oct} = 0.80(1)$
	$B_{F,oct} = 8.7(6)$ Å^2
Goodness-of-fit	$\chi^2 = 1.13$
	3753 experimental data points
	95 Bragg peaks
	10 fitted parameters

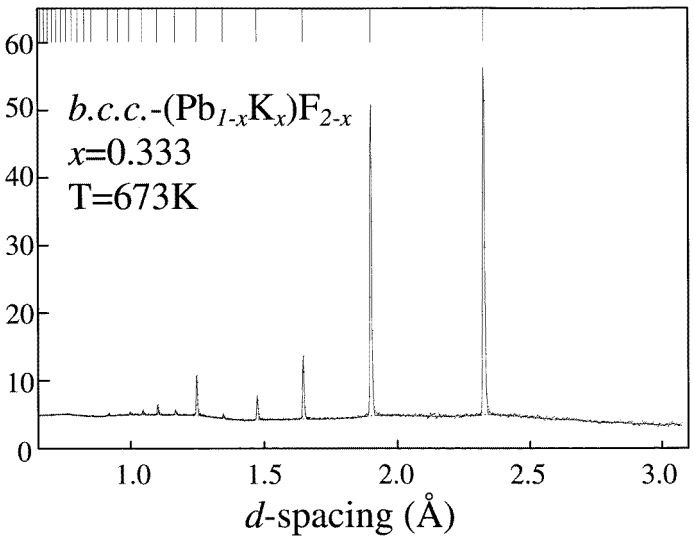

Figure 7. The time-of-flight Rietveld refinement of the diffraction data collected at 673 K and used to determine the structural parameters of the bcc-$(Pb_{1-x}K_x)F_{2-x}$ phase with $x = 0.333$ listed in table 6. The dots are the experimental data points, the line represents the calculated profile and the tick marks at the top of the figure illustrate the expected peak positions.

exceeds the extrinsic vacancy content by a factor $\sim$5 (figure 4) so that the latter are relatively unimportant. As might then be expected, the ionic conductivity for the $x = 0.01$ and $x = 0.0$ samples are very similar at $T >\sim 700$ K. This contrasts with the situation found in many other fluorite structured solid solutions, in which the chemical doping has a profound effect on the ionic conductivity mechanism, superionic transition temperature and structure. Examples include the anion-deficient oxides such as $(ZrO_2)_{1-x}$-$(Y_2O_3)_x$ and anion-excess halides such as $(CaF_2)_{1-x}$-$(YF_3)_x$. However, these systems possess considerably higher

solid solubility limits (typically $x \sim 0.25$–0.35) and are characterized by clusters built up of anion vacancies [36] and interstitials [37]. These defects are known to play a central role in both enhancing [38] and hindering [39] the high-temperature ionic motion. The limited extent of the fluorite solid solution in $(PbF_2)_{1-x}$-$(KF)_x$ is then unlikely to allow the formation of extended defects.

4.2. Comparison with bcc Ag^+ superionics

As discussed previously in section 3.5, the structure of the high-temperature phase of bcc-$(Pb_{1-x}K_x)F_{2-x}$ with $x = 0.333$ can be described as an 'anti α-AgI' arrangement. Pb^{2+} and K^+ are randomly distributed over the 2(a) sites at $(0, 0, 0)$ and $(\frac{1}{2}, \frac{1}{2}, \frac{1}{2})$ and the (highly disordered) anions reside on the tetrahedral and, to a lesser extent, the octahedral interstices formed by the bcc cation sublattice. The significance of the 'anti' nature of the bcc-$(Pb_{1-x}K_x)F_{2-x}$ superionic phase is highlighted by the ionic radii (table 1) because it is the *larger* ionic species which is mobile. In silver based bcc structured superionics the (smaller) mobile Ag^+ are located predominantly on the tetrahedral sites, with no evidence of octahedral occupancy in, for example, α-AgI [4] or γ-Ag_2Te [6]. With reference to figure 6, there are 12 tetrahedral sites available to mobile (M) ions within the unit cell and only two sites for the fixed (X) species. The highest stoichiometry of a bcc structured superionic phase with mobile ions occupying tetrahedral sites is then M_6X. However, geometric effects due to the finite size of the ions do not allow all the tetrahedral sites to be filled simultaneously. Each tetrahedral site has four nearest neighbour (nn) tetrahedral sites at a distance $\sqrt{2}a_0/4$, two next nearest neighbour (nnn) sites at a distance $a_0/2$ and a further eight sites at a distance $\sqrt{6}a_0/4$. If we consider the unit cell constants of α-AgI ($a_0 = 5.05(1)$ Å at 420 K [3]) and γ-Ag_2Te ($a_0 = 5.329(1)$ Å at 1123 K [6]) and the ionic radius of silver ($r^{IV}_{Ag^+} = 1.01$ Å) it follows that no nn sites can be simultaneously filled. The highest possible stoichiometry is then M_3X. This hypothetical arrangement, illustrated in figure 8(a), is expected to be a poor superionic, because a mobile Ag^+ cannot move to an empty tetrahedral site without adopting anomalously short cation–cation distances. Within this simple argument, the presence of empty tetrahedral sites are then compatible with the superionic behaviour observed in the $M = Ag^+$ phases α-AgI and γ-Ag_2Te, because these 'real' compounds have lower cation contents.

4.3. Local order in superionic bcc-$(Pb_{1-x}K_x)F_{2-x}$ with $x = 0.333$

If we now consider the case of bcc-$(Pb_{1-x}K_x)F_{2-x}$ with $x = 0.333$, the distance between the nn tetrahedral sites (1.65 Å) and nnn tetrahedral sites (2.34 Å) are both less than twice the anion ionic radius ($2 \times r^{IV}_F = 2.62$ Å) and the maximum number of anions which can be accommodated on the tetrahedral sites is three per unit cell. This stoichiometry of $M_{1.5}X$ is illustrated in figure 8(b) and, once again, does not allow long-range diffusion of the mobile species. The observation of significant occupancy of octahedral sites in bcc-$(Pb_{1-x}K_x)F_{2-x}$ with $x = 0.333$ (which is equivalent to $XM_{1.667}$) is then a consequence of steric constraints which restrict the occupancy of tetrahedral positions. With reference to the refined values (table 6), there are 2.53(2) anions distributed over the three available tetrahedral sites, with the remaining 0.80(1) located on octahedral holes. However, the tetrahedral sites have four anion–cation distances of 2.61 Å and the octahedral cavities are smaller and somewhat distorted, with 2 cations at a distance 2.33 Å and a further four at 3.30 Å (table 4). It is reasonable then to assume that the smaller Pb^{2+} cations are preferentially located at the shorter distances ($r^{IV}_{Pb^{2+}} + r^{IV}_{F^-} = 2.29$ Å) and the remaining four are occupied, on average,

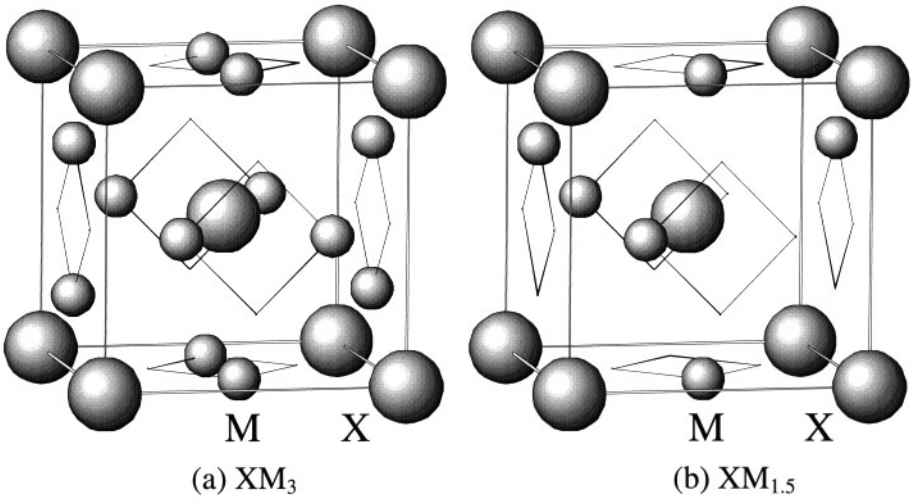

Figure 8. Schematic diagrams of two hypothetical structures with maximum concentration of mobile ions (M) occupying only the tetrahedral sites formed by a bcc sublattice of immobile X ions. Geometric constraints which do not allow nearest neighbour M_{tet} sites to be filled leads to the maximum stoichiometry of XM_3 represented in (a). The additional restriction forbidding the simultaneous occupancy of next-nearest neighbour sites leads to arrangement (b) with stoichiometry $XM_{1.5}$.

by $2 \times Pb^{2+}$ and $2 \times K^{+}$. Similarly, the location of an anion on an octahedral site does not allow any of the neighbouring 12 tetrahedral sites to be filled by other anions.

These considerations lead to a structural model for the local order within the superionic phase of bcc-$(Pb_{1-x}K_x)F_{2-x}$ which is consistent with the refined parameters presented in table 6 and does not include anomalously short anion–anion or anion–cation contacts. This configuration is illustrated in figure 9. The possibilities of ordering of 'mobile' species within a bcc sublattice have been extensively addressed using theoretical [40, 41] and molecular dynamics [42–44] techniques. In the case of α-AgI, Madden *et al* [43] consider the 12(d) tetrahedral sites as 6 interpenetrating bcc arrays, only two of which become occupied as the temperature is lowered. However, these studies considered only tetrahedral sites and, as a consequence, cannot be directly applied to bcc-$(Pb_{1-x}K_x)F_{2-x}$. Instead, we consider the coherent diffuse scattering observed as undulations in the measured 'background' between the Bragg peaks (figure 7). This intensity arises from short-range correlations between disordered ions and its study provides a 'snapshot' picture of the ion positions within the sample. Unfortunately, the limited d-spacing range over which diffraction data were collected do not allow direct analysis of the diffuse scattering by conventional Fourier transform or reverse Monte Carlo methods [45]. Instead, we perform calculations of the coherent diffuse scattering to test the proposed defect model.

The principal features of this approach are now described. A large configuration is generated ($10 \times 10 \times 10$ unit cells in extent), containing $2667 \times Pb^{2+}$, $1333 \times K^{+}$ and $6667 \times F^{-}$ ions. The cations are randomly distributed over the (0, 0, 0) and ($\frac{1}{2}$, $\frac{1}{2}$, $\frac{1}{2}$) sites within the bcc lattice, but each is displaced from its 'ideal' position in a random direction such that, when summed over the whole configuration, the cation distribution has a Gaussian form which models the thermal displacements $B_{Pb/K}$ given in table 6. The required number of anions to be situated on the octahedral sites is then calculated ($6667 \times m_{F,oct}/(m_{F,oct}+m_{F,tet}) = 1600$).

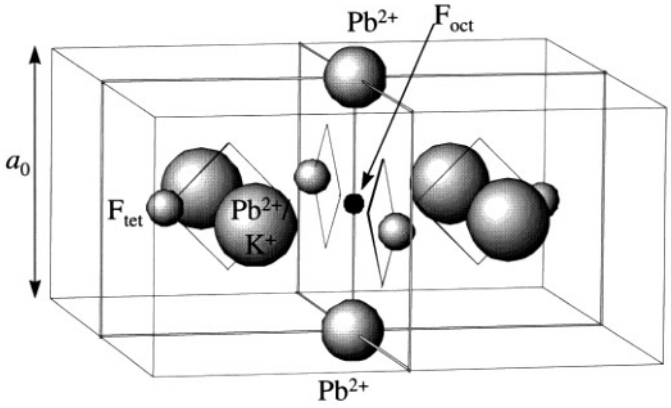

Figure 9. A plausible defect cluster model to explain the presence of F^- on octahedral sites within the superionic phase bcc-$(Pb_{1-x}K_x)F_{2-x}$. An anion can be accommodated on an octahedral site (F_{oct}) if the two nearest neighbour cation sites in [001] directions are occupied by smaller Pb^{2+}. The remaining four surrounding cation sites may be filled by either cation species. Surrounding anions on tetrahedral sites (F_{tet}) cannot occupy the nearest neighbour or next nearest neighbour positions.

Each is, in turn, placed on a randomly chosen (empty) octahedral site, again with a displacement to model the effects of thermal displacement. However, if the anion is in a position that gives anion–cation contacts smaller than the sum of the relevant hard-sphere ionic radii then the site is rejected and another tried. In this manner, F^- tend to preferentially populate the octahedral cavities which have the smaller Pb^{2+} located at the shorter two cation distances ($a_0/2$). Having successfully located all octahedral anions, the remainder are placed randomly over the tetrahedral interstices provided, once again, that they do not produce anomalously short anion–anion or anion–cation distances. Calculation of the neutron scattering intensity against d-spacing using the completed configuration of 10 667 ions will contain both the Bragg and diffuse components. However, the finite size of the assembly of ions will cause the former to be significantly broader than those measured. As a result, we artificially 'remove' the calculated Bragg peaks as follows. Initially, 1000 equally spaced positions in three-dimensional reciprocal space $\boldsymbol{Q} = (Q_h, Q_k, Q_l)$ are chosen, which all have d-spacing of $d = 0.75$ Å (where $d = a_0/\sqrt{Q_h + Q_k + Q_1}$). However, any Q values which lie within the 0.1 reciprocal lattice unit of the location of an allowed Bragg peak are discounted. The scattering function is then calculated over the remaining positions, the average intensity per $\boldsymbol{Q}$ position determined and this procedure repeated at successively higher values of d-spacing up to $d = 8$ Å. In this manner, the variation in the intensity of the coherent diffuse scattering for $0.75 \leqslant d(\text{Å}) \leqslant 8.0$ is calculated.

This approach is rather intensive in its use of computer time and, as a consequence, is not suitable for fitting of the data by refining the parameters which describe the defect model. However, it does allow concepts of physical 'sense' (inter-ionic separations, etc) to be built into the model and directly includes the results of the analysis of the Bragg scattering (positions, occupancies and thermal vibration parameters). As illustrated in figure 10, the calculated variation in the calculated diffuse scattering with d-spacing is in broad agreement with the modulations observed in the experimental diffraction pattern. As a result, we conclude that short-range correlations occur which involve the two cation species *and* the distribution of anions over the octahedral and tetrahedral sites, of the type illustrated in figure 9.

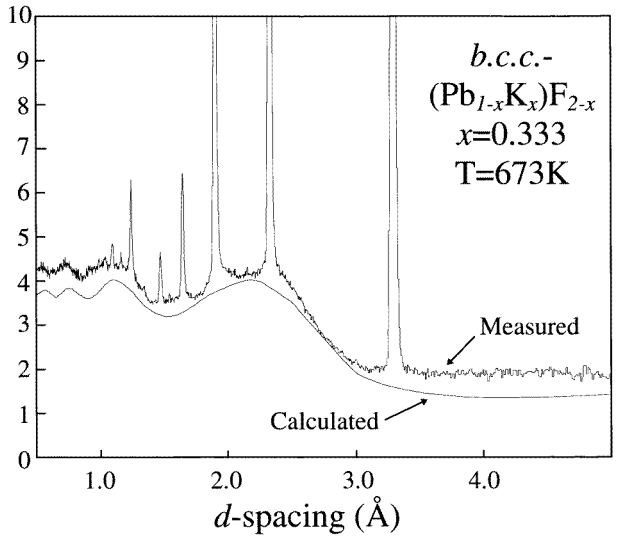

Figure 10. Comparison of the coherent diffuse scattering measured from the phase bcc-$(Pb_{1-x}K_x)F_{2-x}$ with $x = 0.333$ at 673 K with that calculated using defect clusters of the type illustrated in figure 9.

5. Conclusions

The complementary use of impedance spectroscopy and neutron diffraction techniques has provided a direct insight into the structural behaviour and ionic conduction processes in $(PbF_2)_{1-x}$-$(KF)_x$ in the composition range $0.0 \leqslant x \leqslant 0.333$. To the best of our knowledge, the high-temperature phase termed bcc-$(Pb_{1-x}K_x)F_{2-x}$ is the first example of an 'anti-α-AgI' structured superionic. Its study permits an interesting comparison with the more commonly studied Ag^+ and Cu^+ superionics with the bcc structure (α-AgI, α-CuBr and γ-Ag_2Te). In particular, the presence of significant numbers of mobile ions on the octahedral sites is a direct consequence of the size and concentration of F^-. Preliminary studies suggest that the bcc-$(Pb_{1-x}K_x)F_{2-x}$ phase remains stable at higher K^+ concentrations, possibly as far as $x \sim 0.5$–0.6. Further neutron diffraction and impedance spectroscopy studies are planned to investigate the effect of the decreasing anion content on the superionic behaviour of this novel phase.

In the wider context, this observation forms provides a rare example of the similarities between the two major families of superionics—the fluorite structured compounds and the Ag^+/Cu^+ halides. Doping with K^+ changes the superionic transition in PbF_2 from a gradual (type II) to an abrupt (type I) one, such that it closely resembles the behaviour of AgI. It is hoped that experimental studies of this type will motivate further theoretical attempts to unify the description of superionic compounds and to predict *ab initio* the nature of the superionic transition in a given compound (see, for example [46]).

Acknowledgments

We are extremely grateful to J Dreyer, J Bones and R Humphreys for their assistance with the development of the impedance spectroscopy apparatus. One of the authors (PB) wishes

to thank the Swedish Foundation for International Co-operation in Research and Higher Education for financial support.

References

[1] Chandra S 1981 *Superionic Solids. Principles and Applications* (Amsterdam: North-Holland)
[2] Boyce J B and Huberman B A 1979 *Phys. Rep.* **51** 189
[3] Wright A F and Fender B E F 1977 *J. Phys. C: Solid State Phys.* **10** 2261
[4] Nield V M, Keen D A, Hayes W and McGreevy R M 1993 *Solid State Ionics* **66** 247
[5] Bührer W and Hälg W 1977 *Electrochim. Acta* **22** 701
[6] Schneider J and Schulz H 1993 *Z. Kristall.* **203** 1
[7] Keen D A and Hull S 1995 *J. Phys.: Condens. Matter* **7** 5793
[8] Hutchings M T, Clausen K, Dickens M H, Hayes W, Kjems J K, Schnabel P G and Smith C 1984 *J. Phys. C: Solid State Phys.* **17** 3903
[9] Andersen N H, Clausen K and Kjems J K 1983 *Solid State Ionics* **9&10** 543
[10] Goff J P, Hayes W, Hull S and Hutchings M T 1991 *J. Phys.: Condens. Matter* **3** 3677
[11] Schröter W and Nolting J 1980 *J. Phys. Coll.* **41** 20
[12] Oberschmidt J and Lazarus D 1980 *Phys. Rev.* B **21** 2952
[13] Samara G A 1979 *J. Phys. Chem. Solids* **40** 509
[14] Liang C C and Joshi A V 1975 *J. Electrochem. Soc.: Electrochem. Sci. and Techn.* **122** 466
[15] Ito Y, Mukoyama T, Kanamaru F and Yoshikado S 1994 *Solid State Ionics* **73** 283
[16] Bonne R W and Schoonman J 1997 *J. Electrochem. Soc.: Electrochem. Sci. and Techn.* **124** 28
[17] Denes G, Yu Y H, Tyliszczak T and Hitchcock P 1993 *J. Solid State Chem.* **104** 239
[18] Lucat C, Campet G, Claverie J, Portier J, Reau J M and Hagenmuller P 1976 *Mater. Res. Bull.* **11** 167
[19] Reau J M, Federov P P, Rabardel L, Mater S F and Hagenmuller P 1983 *Mater. Res. Bull.* **18** 1235
[20] Meyer A, Ten Eicken J, Glumov O V, Gunsser W, Karus M and Murin I V 1995 *Radiat. Eff. Defects in Solids* **137** 147
[21] Laval J P, Depierrefixe C, Frit B and Roult G 1984 *J. Solid State Chem.* **54** 260
[22] Soubeyroux J L, Reau J M, Matar S, Hagenmuller P and Lucat C 1981 *Solid State Ionics* **2** 215
[23] Reau J M, Yong Jun X, Senegas J and Hagenmuller P 1995 *Solid State Ionics* **78** 315
[24] Kennedy J H and Miles R C 1976 *J. Electrochem. Soc.: Solid State Sci. and Techn.* **123** 47
[25] Schmitz-Dumont O and Bergerhoff G 1956 *Z. Anorg. (Allg.) Chem.* **283** 314
[26] Pistorius C W F T and Van Rensburg J E J 1971 *Z. Anorg. (Allg.) Chem.* **383** 204
[27] Botalov A I and Korenov Y M 1996 *Zh. Neorg. Khim.* **41** 962
[28] Gardner N J G, Hull S, Keen D A and Berastegui P 1998 *Rutherford Appleton Laboratory Technical Report* RAL-TR-1998-032
[29] Smith R I and Hull S 1997 *Rutherford Appleton Laboratory Technical Report* RAL-TR-97-038
[30] David W I F, Ibberson R M and Matthewman J C 1992 *Rutherford Appleton Laboratory Report* RAL-92-032
[31] Brown P J and Matthewman J C 1987 *Rutherford Appleton Laboratory Report* RAL-87-010
[32] Hull S and Wilson C C 1992 *J. Solid State Chem.* **100** 101
[33] Keller H 1976 *Z. Natur. B: Anorg. Chemie.* **31** 885
[34] Müller B G 1982 *Z. Anorg. Allg. Chemie.* **491** 245
[35] Vilminot S and Schulz H 1988 *Acta Crystallogr.* B **44** 233
[36] Hull S, Farley T W D, Hackett M A, Hayes W, Osborn R, Andersen N H, Clausen K, Hutchings K T and Stirling W G 1988 *Solid State Ionics* **28** 488
[37] Hofmann M, Hull S, McIntyre G J and Wilson C C 1997 *J. Phys.: Condens. Matter* **9** 845
[38] Catlow C R A, Comins J D, Germano F A, Harley R T, Hayes W and Owen I B 1981 *J. Phys. C: Solid State Phys.* **14** 329
[39] Catlow C R A 1984 *Solid State Ionics* **12** 67
[40] Szabó G and Kertész J 1986 *J. Phys. C: Solid State Phys.* **19** L273
[41] Szabó G 1986 *J. Phys. C: Solid State Phys.* **19** 3775
[42] O'Sullivan K, Chairotti G and Madden P A 1991 *Phys. Rev.* B **43** 13 536
[43] Madden P A, O'Sullivan K F and Chairotti G 1992 *Phys. Rev.* B **45** 10 206
[44] Seok C and Oxtoby D W 1997 *Phys. Rev.* B **56** 11 485
[45] Keen D A, Hayes W and McGreevy R L 1990 *J. Phys.: Condens. Matter* **2** 2773
[46] Hainovsky N and Maier J 1995 *Phys. Rev.* B **51** 15 789